ISSN 1560-3547, Regular and Chaotic Dynamics, 0000, Vol. 00, No. 0, pp. 1–15. © RCD Editorial Office, 2016.

Synchronization and bistability of two uniaxial spin transfer oscillators with field coupling

Pavel V. Kuptsov[1*]

[1] *Kotelnikov Institute of Radio-Engineering and Electronics of RAS, Saratov Branch*
Zelenaya 38, Saratov, 410019, Russia

Received July 21, 2022; revised Month XX, 20XX; accepted Month XX, 20XX

Abstract—Spin transfer oscillator is a nanoscale device demonstrating self-sustained precession of its magnetization vector whose length is preserved. Thus the phase space of this dynamical system is limited by a three-dimensional sphere. Generic oscillator is described by Landau-Lifshitz-Gilbert-Slonczewski equation, and we consider a particular case of a uniaxial symmetry when the equation yet experimentally relevant is reduced to a dramatically simple form. Established regime of a single oscillator is a purely sinusoidal limit cycle coinciding with a circle of sphere latitude (assuming that points where the symmetry axis passes through the sphere are the poles). On the limit cycle the governing equations become linear with respect to two orthogonal to the axis oscillating components of the magnetization vector while the third one along the axis remains constant. In this paper we analyze how this effective linearity manifests itself when two such oscillators are mutually coupled via their magnetic fields. Using phase approximation approach we reveal that the system can demonstrate bistability between synchronized and non-scrutinized oscillations. For the synchronized one the Adler equation is derived, and the estimates for the boundaries of the bistability area are obtained. The two dimensional slices of basins of attraction of the two coexisting solutions are considered. They are found to be embedded into each other forming a series of parallel stripes. Charts of regimes and Lyapunov exponents charts are computed numerically. Due to the effective linearity the overall structure of the charts is very simple; no higher order synchronization tongues except the main one are observed.

MSC2010 numbers: 34D06,37M05,37M20

DOI: 10.0000/S1560354700000012

Keywords: uniaxial spin transfer oscillators, mutual synchronization, bistability

1. INTRODUCTION

Spin transfer oscillator is a nanoscale device that demonstrates self-sustained oscillations due to the spin-transfer-torque effect from a current with spin polarization that it acquires when passing through a permanent magnet. The angular momentum carried by this current exerts a torque on the magnetization vector of a nanomagnet that results in the magnetization vector precession. The simple configuration of the spin transfer nano-oscillator is shown in Fig. 1. It consist of two ferromagnetic layers separated by a non-magnetic spacer. The lower "fixed" layer is relatively thick so that its magnetization $\vec{p}$ remains constant. The upper one is thin and thus "free": its magnetization $\vec{m}$ can be changed. Downward current density $\vec{j}$ corresponds to the upward electron flow that passes the fixed layer first acquiring spin polarization. Then the flow comes to the free layer and excited its magnetization $\vec{m}$ oscillations due to the spin-transfer-torque effect. Also an external magnetic field $\vec{h}_{\text{ext}}$ can be applied. More details of physical implementation of this device can be found in Refs. [1, 2].

First theoretical description of how to modify a magnetization of nanomagnets via the spin-transfer-torque effect from a spin-polarized current was suggested by Slonczewski [3] and Berger [4] in 1996. This is based on the Landau-Lifshitz-Gilbert equation that describes magnetization dynamics in ferromagnets in the presences of precession damping. Spin-transfer-torque effect is

*E-mail: p.kuptsov@rambler.ru

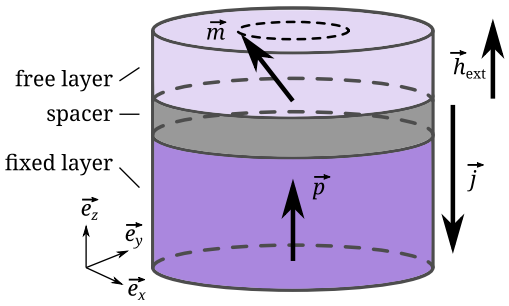

Fig. 1. Spin transfer nano-oscillator. Fixed layer is a thick ferromagnet with permanent magnetization $\vec{p}$. Free layer is a relatively thin ferromagnet whose magnetization can easily be changed. Spacer is non-magnetic layer made of insulator or non-magnetic metal. Current density vector $\vec{j}$ is downward so that the upward electron flow passes the fixed layer first acquiring there the spin polarization and then excites oscillating magnetization $\vec{m}$ of the free layer due to spin-transfer-torque effect. Also an external magnetic field $\vec{h}_{\text{ext}}$ can be applied.

taken into account by adding a term that is now known as Slonczewski spin-transfer torque [3]. The resulting Landau-Lifshitz-Gilbert-Slonczewski in the dimensionless form reads [1]

$$\dot{\vec{m}} - \alpha\vec{m}\times\dot{\vec{m}} = -\vec{m}\times\vec{h}_{\text{eff}} + \frac{\beta}{1+c_p(\vec{m}\cdot\vec{p})}\,\vec{m}\times(\vec{m}\times\vec{p}). \tag{1.1}$$

Here "$\cdot$" and "$\times$" denote dot and cross products, respectively, $\vec{m}$ is a unit vector representing oscillating magnetization in the free layer, $\vec{p}$ is also a unit vector indicating constant magnetization direction in the fixed layer, α is a parameter controlling the Gilbert damping of the spin precession, β is proportional to the current density j. The effective magnetic field $\vec{h}_{\text{eff}}$ is the sum of the external, demagnetizing and anisotropy fields (see [1, 5] for more details). Accepting a physically reasonable assumption that the free layer is a flat ellipsoid, and that the crystal anisotropy is uniaxial in character, with the anisotropy axis parallel to one of the principal axes of the ellipsoid, see book [1] as well as many other publications, e.g. [6–10], where this assumption is utilized, one can write the effective field as

$$\vec{h}_{\text{eff}} = \vec{h}_{\text{ext}} - \mathcal{D}\vec{m}, \tag{1.2}$$

where $\mathcal{D}$ is a diagonal anisotropy tensor and $\vec{h}_{\text{ext}}$ is the external field. Coefficient c_p in Eq. (1.1) depends on physical properties of the considered nano-devices as well as on the degree of the spin polarization of the current. It may attain values in the interval $-1 < c_p < 1$ [1]. Often in theoretical studies it is assumed that $c_p = 0$, see e.g. [6–10]. In what follows we will also accept this assumption.

Straightforward vector algebra shows that $\dot{\vec{m}}\cdot\vec{m} = 0$. It means that an arbitrary initial norm of $\vec{m}$ will be preserved in time. Since Eq. (1.1) is obtained after normalization of the free layer magnetization by its saturation value [1] the initial vector $\vec{m}(t=0)$ will always be taken of the unit norm so that $\|\vec{m}(t)\| = 1$ for any t.

Since the generation of spin transfer oscillators was observed experimentally [11, 12] a lot of attention has been attracted to a collective behavior of the coupled oscillators. The coupling between spin transfer oscillators is usually introduced either through common current or via magneto-dipolar field. Coupling via common current means that the devices are connected in parallel or in series. Due to giant magnetoresistance effect their resistance oscillates along with the magnetization. It results in the current variation that in turn influences back the oscillations [6, 7, 9, 10].

In this paper we consider the second type of coupling when the magnetic field of one oscillator influences another oscillator and vice versa. Such sort of coupling is implemented experimentally [13] as well as theoretically [14, 15]. In paper [16] amplitude equation is derived for the coupled spin-transfer oscillators and the field coupling is also considered.

The main point of interest in studying of coupled spin transfer oscillators are phase locking by external forcing and mutual synchronization if two or more oscillators are coupled. These effects are known to be typical for systems with self-sustained oscillations [17]. Besides the fundamental interest, synchronization of spin transfer oscillators is important for practical applications since a single oscillator has rather weak output power [18].

Papers [6, 7] analyze synchronization of an array of spin transfer oscillators coupled via common current and describe multistability when non-synchronous regimes coexist with fully synchronized oscillations. As a result this complete synchronization is not always develops from random initial state. In many cases nontrivial clustering is observed including quasiperiodic and chaotic states. In more detail the complex clustering is analyzed in [9]. Various regimes of different level of complexity, including chimeras, are discussed. Paper [10] demonstrates that the lack of full synchronization of the spin transfer oscillators can be a result of proximity to the homoclinicity. A noise added to a system in this situation can suppress precession of all oscillators.

In this paper we consider particular form of a spin transfer oscillator when it has uniaxial symmetry. This case yet practically relevant is described by dramatically simpler equations as compared to the generic form (1.1). Two such oscillators coupled via magnetic fields are found to have no higher resonances in their parameter space except the main one were the frequencies ratio is $1:1$. Thereby the parameter space has a very simple structure: there are areas of two types, one for fully synchronized regime and another for non-synchronized oscillations. Similarly to the case reported for common current coupling [6, 7] the bistability is observed. For a certain range of coupling parameter the two solutions coexist, the synchronized and non-synchronized ones. Their basins of attraction in the phase space, as observed on the two dimensional slices, are embedded into each other: the slices consist of sufficiently thin parallel stripes. Small variation of the initial conditions can result in regime switch from synchronization to non-synchronized oscillations.

2. SINGLE OSCILLATOR WITH UNIAXIAL SYMMETRY

We are going to consider practically important but yet simple particular case of the uniaxial symmetry around z-axis [1]:

$$\vec{h}_{\text{eff}} = h_z\vec{e}_z - m_z\vec{e}_z,\ \vec{p} = \vec{e}_z, \tag{2.1}$$

where the diagonal elements of $\mathcal{D}$ are reduced to $(0, 0, 1)$ and h_z is the only nonzero component of the external field $\vec{h}_{\text{ext}}$. In this case Eq. (1.1) takes the form:

$$\begin{aligned}(1+\alpha^2)\dot{m}_x =& m_z A m_x + B m_y,\\ (1+\alpha^2)\dot{m}_y =& -B m_x + m_z A m_y,\\ (1+\alpha^2)\dot{m}_z =& A(m_z^2 - 1),\end{aligned} \tag{2.2}$$

$$A = (m_z - h_z + \beta/\alpha)\alpha,\ \ B = m_z - h_z - \beta\alpha, \tag{2.3}$$

where m_x, m_y, m_z are components of a vector $\vec{m}$. This system has three control parameters: α is responsible for precession damping and depends on the oscillator material properties, β is proportional to the current density that flows through the oscillator and h_z is an externally applied magnetic field.

Dynamics of the uniaxial oscillator (2.2) is considered in detail in [1]. We discuss it only in brief. Equations (2.2) are split into two subsystems since m_z does not depend on m_x and m_y. Equation for m_z has three fixed points: $m_z = \pm 1$ and $m_z = h_z - \beta/\alpha$, and only one of them can be stable as follows from their linear stability analysis [1]. Solutions corresponding to $m_z = \pm 1$ imply that $m_x = m_y = 0$ and thus are non-oscillatory. Conditions of their stability are

$$\begin{aligned} m_z =& -1 \quad \text{at } h_z - \beta/\alpha < -1,\\ m_z =& 1 \qquad \text{at } h_z - \beta/\alpha > 1.\end{aligned} \tag{2.4}$$

The oscillatory solution corresponds to the third fixed point:

$$m_z = h_z - \beta/\alpha \quad \text{at } -1 < h_z - \beta/\alpha < 1. \tag{2.5}$$

When m_z approaches one of the fixed points (2.4) or (2.5) it varies slowly so that we can neglect its variation in equations for m_x and m_y and solve them as follows:

$$m_x = r\mathrm{e}^{m_z A t}\cos Bt,\ m_y = -r\mathrm{e}^{m_z A t}\sin Bt, \tag{2.6}$$

where r depends on m_z according to the condition $m_x^2 + m_y^2 + m_z^2 = 1$. When either $m_z = 1$ or $m_z = -1$ is stable, see Eq. (2.4), the exponent is negative, $m_z A < 0$, and m_x and m_y decay to

zero while rotating around z axis. These fixed points are stable focuses. When $m_z = h_z - \beta/\alpha$ is stable, see Eq. (2.5), the exponent $m_z A$ is positive near $m_z = \pm 1$ so that these fixed points are now unstable focuses. The exponent vanishes as m_z approaches $h_z - \beta/\alpha$. As a result at this point the stationary oscillatory solution is

$$m_x = \sqrt{1-a^2}\cos(\omega t + f),\ m_y = \sqrt{1-a^2}\sin(\omega t + f),\ m_z = a, \tag{2.7}$$

where f is a constant that depends on the initial conditions and the eigenfrequency ω and the stationary amplitude a of the oscillator are

$$\omega = \beta/\alpha, \tag{2.8}$$

$$a = h_z - \beta/\alpha. \tag{2.9}$$

It should be noted that Eq. (2.7) is an exact stationary solution of the uniaxial oscillator (2.2). This solution is pure sinusoidal, without harmonics, and oscillating subsystem of Eq. (2.2) is linear with respect to m_x and m_y. It means that when this system is forced periodically or interacts with another oscillating system no higher order resonances are possible at least when the interaction is not very strong. This is due to the fact that the perturbation transfer mechanism between harmonics occurs via nonlinearity and this is effectively absent. More complicated regimes can be expected, if any, only when the interaction produces an essential perturbation to m_z.

3. FIELD COUPLING

We will consider oscillators coupled via magnetic fields in dipole approximation. In this case the field is assumed to be proportional to the magnetization of the oscillators and the coupling term for the nth oscillator is introduced as a correction to the effective field (c.f. Eq. (1.2)):

$$\vec{h}_{\text{eff},n} = \vec{h}_{\text{ext}} - \mathcal{D}\vec{m}_n + \epsilon \sum_{j=1, j\neq n}^{N} a_{n,j}\vec{m}_j. \tag{3.1}$$

Here $\vec{m}_j$ is magnetization of the jth oscillator in an ensemble and ϵ is the coupling strength. Coefficients $a_{n,j} \in [0,1]$ determine the structure of couplings.

Assuming the effective filed to be given by Eq. (3.1) we can write the Landau-Lifshitz-Gilbert-Slonczewski equations for a network of spin-transfer oscillators as follows (as already mentioned above $c_p = 0$):

$$\dot{\vec{m}}_n - \alpha\vec{m}_n \times \dot{\vec{m}}_n = -\vec{m}_n \times \vec{h}_{\text{eff},n} + \beta_n\, \vec{m}_n \times (\vec{m}_n \times \vec{p}). \tag{3.2}$$

Coefficients $a_{n,j}$ in Eq. (3.1) form an adjacency matrix of the oscillator network. Since $\vec{h}_{\text{eff},n}$ appears in Eq. (3.2) as a part of the cross product with $\vec{m}_n$ the diagonal elements $a_{n,n}$ vanish due to the identity $\vec{m}_n \times \vec{m}_n = 0$. Values of $a_{n,j}$ depend on the decay rate of the magnetic field between oscillators. For example a dipole field falls off as the inverse cube of the distance [19]. Since the filed propagates as an electromagnetic wave, filling the area between oscillators with an absorbing medium one can obtain an exponential decay. Thus selecting the oscillator configuration one needs to take into account their geometrical locations. Moreover due to sufficiently fast falling of the fields it is natural to assume that the coupling strength ϵ is rather small.

Similarly to the single oscillator (1.1) each oscillator vector $\vec{m}_n$ in the network (3.2) preserves its length, $\|\vec{m}_n(t)\| = 1$. This can be checked directly by computing the dot product $\dot{\vec{m}}_n \cdot \vec{m}_n$ that remains zero for any t.

4. TWO COUPLED OSCILLATORS. PHASE APPROXIMATION ANALYSIS

Consider two oscillators coupled according to the scheme discussed in Sec. 3. Equations for the first one reads

$$\begin{aligned}(1+\alpha^2)\dot{m}_{1,x} =& m_{1,z}A_1 m_{1,x} + B_1 m_{1,y} + \\ & \epsilon\left\{\alpha[m_{2,x} - (\vec{m}_1\cdot\vec{m}_2)m_{1,x}] - m_{1,y}m_{2,z} + m_{2,y}m_{1,z}\right\},\\ (1+\alpha^2)\dot{m}_{1,y} =& -B_1 m_{1,x} + m_{1,z}A_1 m_{1,y} + \\ & \epsilon\left\{\alpha[m_{2,y} - (\vec{m}_1\cdot\vec{m}_2)m_{1,y}] + m_{1,x}m_{2,z} - m_{2,x}m_{1,z}\right\},\\ (1+\alpha^2)\dot{m}_{1,z} =& A_1(m_{1,z}^2-1) + \\ & \epsilon\left\{\alpha[m_{2,z} - (\vec{m}_1\cdot\vec{m}_2)m_{1,z}] - m_{1,x}m_{2,y} + m_{2,x}m_{1,y}\right\},\end{aligned} \tag{4.1}$$

$$A_1 = (m_{1,z} - h_z + \beta_1/\alpha)\alpha,\ \ B_1 = m_{1,z} - h_z - \beta_1\alpha. \tag{4.2}$$

Equations for the second oscillator are obtained by the index exchange $1 \leftrightarrow 2$. The full equations set for two oscillators have five control parameters. We assume that the damping α, the magnetic field h_z and the coupling strength ϵ are the same for both oscillators and they have different current densities that are incorporated into β_1 and β_2, respectively.

These equations can be rewritten via spherical coordinates

$$m_{1,2,x} = \sin\theta_{1,2}\cos\phi_{1,2},\ \ m_{1,2,y} = \sin\theta_{1,2}\sin\phi_{1,2},\ \ m_{1,2,z} = \cos\theta_{1,2}. \tag{4.3}$$

Since oscillations occur basically in xy-plane variables $\phi_{1,2}$ play the role of phases and $\theta_{1,2}$ correspond to the amplitudes. Each oscillator is symmetric with respect to rotation around z axis. Thus the equations in spherical coordinates can be written with respect to the phase difference $\psi = \phi_1 - \phi_2$ and the amplitudes θ_1 and θ_2:

$$\begin{aligned}(1+\alpha^2)\dot{\psi} =& \cos\theta_2 - \cos\theta_1 + \alpha(\beta_1-\beta_2) + \epsilon\big(\cos\theta_2 - \cos\theta_1 \\ & -\alpha\sin\psi[\csc\theta_1\sin\theta_2 + \sin\theta_1\csc\theta_2] + \cos\psi[\sin\theta_1\cot\theta_2 - \cot\theta_1\sin\theta_2]\big),\end{aligned} \tag{4.4a}$$

$$(1+\alpha^2)\dot{\theta}_1 = \big(\alpha\cos\theta_1 + \beta_1 - \alpha h_z\big)\sin\theta_1 + \epsilon\big([\alpha\cos\psi\cos\theta_1 - \sin\psi]\sin\theta_2 - \alpha\sin\theta_1\cos\theta_2\big), \tag{4.4b}$$

$$(1+\alpha^2)\dot{\theta}_2 = \big(\alpha\cos\theta_2 + \beta_2 - \alpha h_z\big)\sin\theta_2 + \epsilon\big([\alpha\cos\psi\cos\theta_2 + \sin\psi]\sin\theta_1 - \alpha\sin\theta_2\cos\theta_1\big). \tag{4.4c}$$

Here $\csc\theta = 1/\sin\theta$ and $\cot\theta = \cos\theta/\sin\theta$ denote cosecant and cotangent functions, respectively. Equations (4.4) do not depend on particular phases $\phi_{1,2}$ and can be solved separately. Equations for $\phi_{1,2}$ is coupled with Eqs. (4.4) in a unidirectional way and are not coupled with each other:

$$(\alpha^2+1)\dot{\phi}_1 = -\cos\theta_1 + h_z + \alpha\beta_1 + \epsilon\left(\cos\theta_2 - [\alpha\sin\psi + \cos\psi\cos\theta_1]\sin\theta_2\csc\theta_1\right), \tag{4.5a}$$

$$(\alpha^2+1)\dot{\phi}_2 = -\cos\theta_2 + h_z + \alpha\beta_2 + \epsilon\left(\cos\theta_1 + [\alpha\sin\psi - \cos\psi\cos\theta_2]\sin\theta_1\csc\theta_2\right). \tag{4.5b}$$

Equations (4.4) have a fixed point solution

$$\psi = \text{const},\ \theta_1 = \theta_2 = \theta = \text{const}, \tag{4.6}$$

that corresponds to the regime of full synchronization of the oscillators: the phases ϕ_1 and ϕ_2 are locked so that the their difference ψ remains constant and the amplitudes θ_1 and θ_2 coincide and are also constant. Substituting (4.6) to Eqs. (4.4) we obtain stationary solutions for ψ and θ:

$$\sin\psi = \frac{\beta_1-\beta_2}{2\epsilon}, \tag{4.7a}$$

$$\cos\theta = \frac{\left(\sqrt{4\epsilon^2 - (\beta_1-\beta_2)^2} + 2\epsilon - 2\right)(2\alpha h_z - \beta_2 - \beta_1)}{\alpha\left(8\epsilon - [\beta_1-\beta_2]^2 - 4\right)}. \tag{4.7b}$$

When the eigenfrequencies of the oscillators (2.8) are close to each other, i.e., $(\beta_1 - \beta_2)$ is small, Eq. (4.7b) is reduced via Taylor series expansion to the form

$$\cos\theta = h_z - \frac{\beta_1+\beta_2}{2\alpha} + O\left((\beta_1-\beta_2)^2\right). \tag{4.8}$$

This is the mean value of stationary amplitudes for the uncoupled oscillators, see Eq. (2.7). Substituting stationary solution (4.7) to the equations for phases (4.5) we obtain $\dot{\phi}_1 = \dot{\phi}_2 = \omega_s$, where

$$\omega_s = \frac{\beta_1 + \beta_2}{2\alpha}. \tag{4.9}$$

Here ω_s is a frequency of the synchronized oscillations. Observe that it is equal to the mean frequencies of the partial oscillators, see Eq. (2.8).

Synchronized solution can be analyzed using phase approximation. When the system is not so far from the limit cycle corresponding to the synchronous regime the amplitudes of the subsystems are close to the amplitudes on the cycle. Thus given the equations describing the dynamics in terms of phases and amplitudes we can substitute the amplitudes on the cycle into the equations and consider phase dynamics only. The phase equation taking into account the first order terms in the coupling strength is called Adler equation. It was first obtained by Adler [20] for a particular system, and later a general method of analysis of dynamical systems that include derivation of the phase equation was developed by Khokhlov [21, 22]. Discussion and description of this method of analysis can be found in the book [17] and its higher order generalization is considered in [23, 24].

Adler equation for our system is derived from Eq. (4.4a) after the substitution $\theta_1 = \theta_2 = \theta$. The terms including θ are canceled so that the equation for ψ acquires the form

$$\dot{\psi} = \delta - \mu \sin\psi, \tag{4.10}$$

where

$$\delta = \left(\frac{\alpha^2}{\alpha^2+1}\right)\frac{\beta_1 - \beta_2}{\alpha}, \;\; \mu = \left(\frac{\alpha^2}{\alpha^2+1}\right)\frac{2\epsilon}{\alpha}. \tag{4.11}$$

Equation (4.10) is a universal model of phase locking for a weakly interacting rotators. Parameter μ in this equation is the coupling strength and δ is the frequency detuning (we recall that the eigenfrequency of a single oscillator is $\beta_{1,2}/\alpha$, see (2.8)).

One-dimensional Eq. (4.10) has fixed points given by Eq. (4.7a). They exists when the right hand side in Eq. (4.7a) is less then 1. When this condition is fulfilled Eq. (4.7a) gives two values for stationary phase differences on the interval $[0, 2\pi]$, one of them always stable. The later corresponds to the synchronized solution. It exists at

$$\epsilon \geq |\beta_1 - \beta_2|/2. \tag{4.12}$$

Now we will use phase approximation to consider an oscillatory solution of Eqs. (4.4) that corresponds to non-synchronous oscillations of the coupled spin-transfer oscillators. Following ideas from [17, 23, 24] we consider time dependent amplitudes $\theta_{1,2}$ as a power series in ϵ restricting ourselves to the first order terms:

$$\theta_1(t) = \theta_1^{(0)} + \epsilon\theta_1^{(1)}(t), \; \theta_2(t) = \theta_2^{(0)} + \epsilon\theta_2^{(1)}(t). \tag{4.13}$$

Here zero order terms $\theta_{1,2}^{(0)}$ correspond to the uncoupled oscillators and thus are constant, see Eq. (2.9).

Substituting expansion (4.13) to Eqs. (4.4b) and (4.4c) and equating terms of the same orders in ϵ we obtain the zero order amplitudes as

$$\cos\theta_1^{(0)} = Z_1, \; \cos\theta_2^{(0)} = Z_2, \; \sin\theta_1^{(0)} = Q_1, \; \sin\theta_2^{(0)} = Q_2. \tag{4.14}$$

where

$$Z_{1,2} = h_z - \beta_{1,2}/\alpha, \; Q_{1,2} = \sqrt{1 - Z_{1,2}^2}. \tag{4.15}$$

For the time dependent first order terms we derive ODEs as follows:

$$\begin{aligned}(\alpha^2+1)\dot{\theta}_1^{(1)} &= -\alpha Q_1^2\theta_1^{(1)} - Q_2\sin\psi + \alpha Q_2 Z_1\cos\psi - \alpha Q_1 Z_2,\\ (\alpha^2+1)\dot{\theta}_2^{(1)} &= -\alpha Q_2^2\theta_2^{(1)} + Q_1\sin\psi + \alpha Q_1 Z_2\cos\psi - \alpha Q_2 Z_1.\end{aligned} \tag{4.16}$$

Equations (4.16) are linear and indendent from each other. They are non-autonomous because we now assume that the phase difference ψ depends on time. The coefficients at $\theta^{(1)}_{1,2}$ are negative so that there is no exponential growth and the solution can be found as

$$\theta^{(1)}_{1,2} = a_{1,2}\cos\psi + b_{1,2}\sin\psi + c_{1,2}. \tag{4.17}$$

Substituting it to Eqs. (4.16) and collecting terms at $\sin\psi$ and $\cos\psi$ we obtain equations for the coefficients $a_{1,2}$, $b_{1,2}$ and $c_{1,2}$. These equations include time derivatives of ψ that can be obtained after substitution (4.13) to Eq. (4.4a) and keeping only zero order terms in ϵ (other terms will go to higher order equations for $\theta^{(n)}_{1,2}$):

$$\dot\psi = (\beta_1 - \beta_2)/\alpha. \tag{4.18}$$

Using this $\dot\psi$ we can solve equations for the coefficients to obtain

$$\begin{aligned}
a_1 &= \frac{Q_2[(Z_2 - Z_1^3)\alpha^2 - (Z_1 - Z_2)]}{(Z_1 - Z_2)^2(\alpha^2+1)^2 + Q_1^4\alpha^2}, & a_2 &= \frac{Q_1[(Z_1 - Z_2^3)\alpha^2 + (Z_1 - Z_2)]}{(Z_1 - Z_2)^2(\alpha^2+1)^2 + Q_2^4\alpha^2},\\
b_1 &= \frac{\alpha Q_2[(Z_1Z_2 - 1) - Z_1(Z_1 - Z_2)\alpha^2]}{(Z_1 - Z_2)^2(\alpha^2+1)^2 + Q_1^4\alpha^2}, & b_2 &= \frac{\alpha Q_1[(Z_1Z_2 - 1) + Z_2(Z_1 - Z_2)\alpha^2]}{(Z_1 - Z_2)^2(\alpha^2+1)^2 + Q_2^4\alpha^2},\\
c_1 &= -Z_2/Q_1, & c_2 &= -Z_1/Q_2.
\end{aligned} \tag{4.19}$$

Now we turn to equation for ψ: substitute the expansion (4.13) to Eq. (4.4a) preserving terms up to the first order in ϵ, and take into account solutions for $\theta^{(0)}_{1,2}$ and $\theta^{(1)}_{1,2}$, see Eqs. (4.14), (4.15), (4.17), (4.19). The resulting equation reads:

$$\dot\psi = \delta_1 - \sqrt{\nu_1^2 + \mu_1^2}\sin(\psi + \gamma), \tag{4.20}$$

where

$$\begin{aligned}
\delta_1 =& 2(\beta_1 - \beta_2)/\alpha,\\
\nu_1 =& \epsilon\frac{Q_2^2Z_1 - Q_1^2Z_2 + Q_1Q_2(Q_2a_2 - Q_1a_1)}{Q_1Q_2(\alpha^2+1)},\\
\mu_1 =& \epsilon\frac{\alpha(Q_2^2 + Q_1^2) - Q_1Q_2(Q_2b_2 + Q_1b_1)}{Q_1Q_2(\alpha^2+1)},
\end{aligned} \tag{4.21}$$

and $\gamma = \arctan(\nu_1/\mu_1)$.

Equation (4.20) is derived using $\theta^{(1)}_{1,2}$ that in turn are obtained with the assumption that ψ depends on time, see Eq. (4.18). Thus Eq. (4.20) makes sense in the domain where it does not have fixed points. Otherwise one of them will always be stable and ψ will arrive at it. It gives the existence condition for a non-synchronous solution:

$$\delta_1^2/(\nu_1^2 + \mu_1^2) > 1. \tag{4.22}$$

To obtain this condition explicitly we substitute here (4.21) and solve it for ϵ. The resulting expression is cumbersome, and below we provide its Taylor series decomposition up to the third order in frequency detuning $\beta_1 - \beta_2$:

$$\epsilon < |\beta_1 - \beta_2| + 8|\beta_1 - \beta_2|^3\,\frac{\alpha^2(1 - 4h_z^2) + 4\alpha(\beta_1 + \beta_2)h_z - (\beta_1 + \beta_2)^2 + 1}{[(2\alpha h_z - \beta_1 - \beta_2)^2 - 4\alpha^2]^2}. \tag{4.23}$$

One more condition for the non-synchronized solution to exist is $Z_{1,2}^2 < 1$:

$$-1 < h_z - \beta_{1,2}/\alpha < 1. \tag{4.24}$$

Otherwise $Q_{1,2}$ becomes imaginary, see Eq. (4.15). We note that it coincides with the condition (2.5) that requires for each separate oscillator to have stable oscillatory solution.

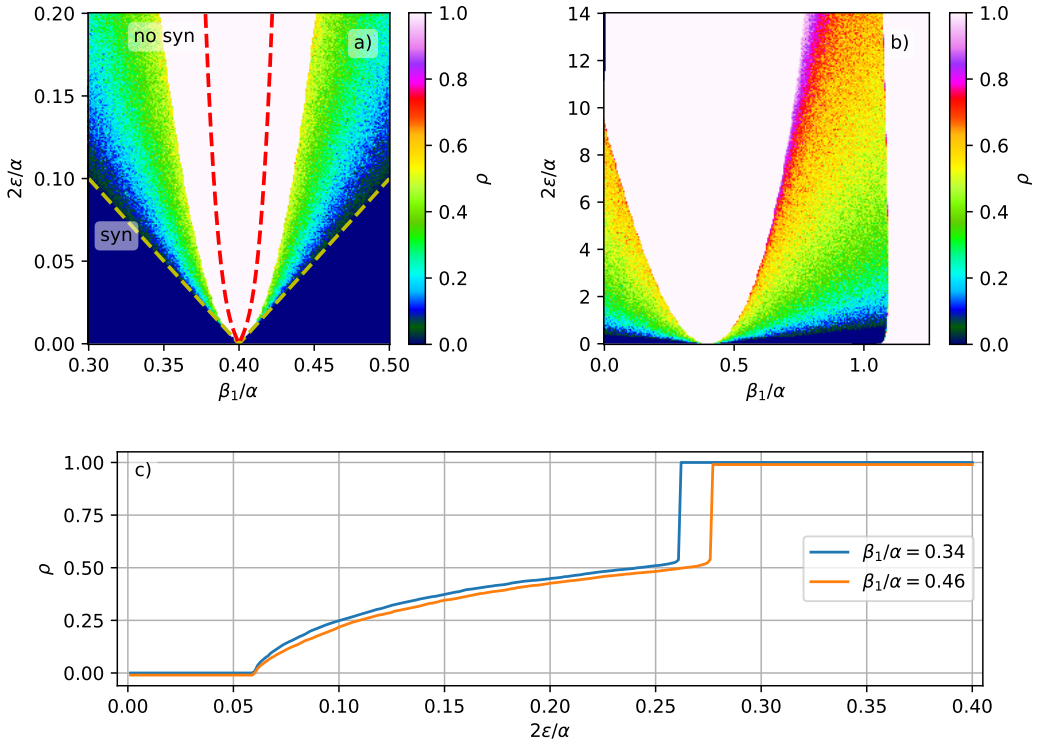

Fig. 2. Density ρ of initial points leading to the synchronized solution. In panel (a) colors encode density values in a small vicinity of the point $\beta_1 = \beta_2$ and panel (b) shows wider ranges for β_1 and ϵ. $\beta_2 = 0.004$, $\alpha = 0.01$, $h_z = 0$. In panel (a) a dashed yellow line 'syn' marks the theoretical lower boundary of the area where the synchronized solution exists, see Eq. (4.12). Dashed red line 'no syn' marks an upper boundary for the non-synchronized solution as estimated by Eq. (4.23). (c) Density of initial points leading to synchronized solution vs ϵ. Parameters are as above except β_1 that are shown in the legend.

To summarize, we have analyzed the fixed point and the oscillatory solution of Eqs. (4.4). They correspond to synchronized and non-synchronized regimes of the considered oscillators, respectively. The ranges in ϵ of their existence obtained in phase approximation are represented by inequalities (4.12) and (4.23). It can be shown that the numerator of the term at $|\beta_1 - \beta_2|^3$ in (4.23) is always positive. On substitution average amplitude $Z = h_z - (\beta_1 + \beta_2)/\alpha$ instead of $(\beta_1 + \beta_2)$ the numerator is reduced to $-4Z^2\alpha^2 + \alpha^2 + 1$. This expression is positive at $Z = 0$ and becomes negative at $Z = \sqrt{\alpha^2 + 1}/(2\alpha)$. Since typically $\alpha \approx 0.01$ this value of the amplitude is very large and physically irrelevant. Altogether it means that the areas of existence of the two solutions overlap, i.e., there is a bistability of synchronous and non-synchronous oscillations.

We note that according to Eq. (4.17) θ_1 and θ_2 both depend on ψ, i.e., oscillate synchronously. Thus in the regime that we call non-synchronous $m_{1,2,x}$ and $m_{1,2,y}$ components are not synchronized since their phase difference ψ is non-stationary and $m_{1,2,z}$ oscillate synchronously.

5. NUMERICAL ANALYSIS

Figure 2 demonstrates numerical verification of the bistability. Color of points in the parameter planes 2a and 2b represent the density ρ of trajectory initial points in the phase space that end up at synchronous regime. Figure 2a is plotted for a small vicinity near the resonance point $\beta_1 = \beta_2$. Here the deep blue color in the lower part depicts an area where only the non-synchronized solution exists. A boundary of the bistability with the synchronized solution is marked by dark green points above the deep blue area. Theoretical yellow dashed lines plotted in accordance with Eq. (4.12) correspond to this numerically obtained boundary very well. The numerically obtained upper boundary of the bistability in Fig. 2a is located on the lower edges of the white tongue-like area. The theoretical

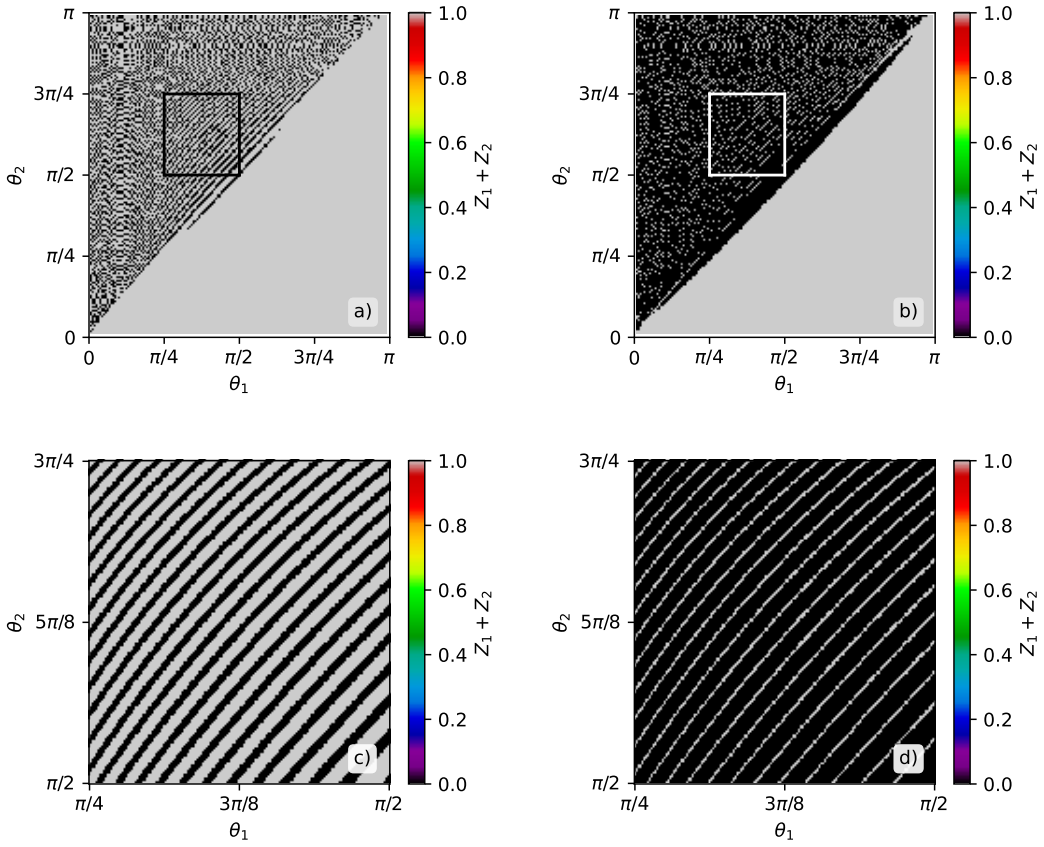

Fig. 3. (a,b) Sum of spans of z components $Z_{1,2} = \max_t m_{1,2,z} - \min_t m_{1,2,z}$ measured when trajectories are issued from different initial points: $m_{1,2,x} = \sin\theta_{1,2}\cos\phi_{1,2}$, $m_{1,2,y} = \sin\theta_{1,2}\sin\phi_{1,2}$, $m_{1,2,z} = \cos\theta_{1,2}$, $\phi_1 = 0$, $\phi_2 = 0.3\pi$. The sums $Z_1 + Z_2$ are normalized by the maximum value. Color gradient is employed for the drawing, however one can see either zeros (black) or ones (gray) points that reveals only two different solutions, like in Figs. 4 and 5, respectively. $\alpha = 0.01$, $\beta_1 = 0.0046$, $\beta_2 = 0.004$, $h_z = 0$. $\epsilon = 0.00045$, and 0.001 for panels (a) and (b), respectively. (c) and (d) Enlarged areas of the panels (a) and (b), respectively, highlighted there by rectangles.

formula for this boundary (4.23) overestimates it, see the red dashed curves. The reason is that it was obtained only for the first order approximation in ϵ.

Figure 2b demonstrates wide ranges of parameters. We again observe the white tongue whose tip is located at the point $\beta_1 = \beta_2$. Within this tongue there is only synchronized solution. Colorful areas below it and above the deep blue points at the bottom correspond to bistability. The white area in the right part represents the situation when the non-synchronized solution does not exists due to the violation of condition (4.24). We note that the theoretically predicted boundary coincides with numerical one for small ϵ. Better estimate could be obtained using higher order decomposition in ϵ.

Figure 2c demonstrates the density ρ vs the coupling strength ϵ. We see that when the coupling is weak the density is zero, $\rho = 0$. It means that no bistability occurs. All solutions are non-synchronous. When the coupling gets larger the density becomes nonzero. This is the range of bistability. Within this range $0 < \rho < 0.5$. Then when the density reaches the level $\rho = 0.5$ it jumps up to $\rho = 1$. In the other words the bistability vanishes when one half of initial points in the phase space lead to the synchronized oscillation.

Figures 3a and 3b reveal basins of attraction of the synchronized and non-synchronized solutions of the system (4.1). As we discussed above, due to the norm preservation $\|\vec{m}_1\| = \|\vec{m}_2\| = 1$ and because of the symmetry with respect to z axis the system can be described by the three ODEs for θ_1, θ_2 and $\psi = \phi_1 - \phi_2$, see Eqs. (4.4). We keep initial ψ constant (the particular value does not influence the qualitative picture) and start trajectories from points with various θ_1 and θ_2.

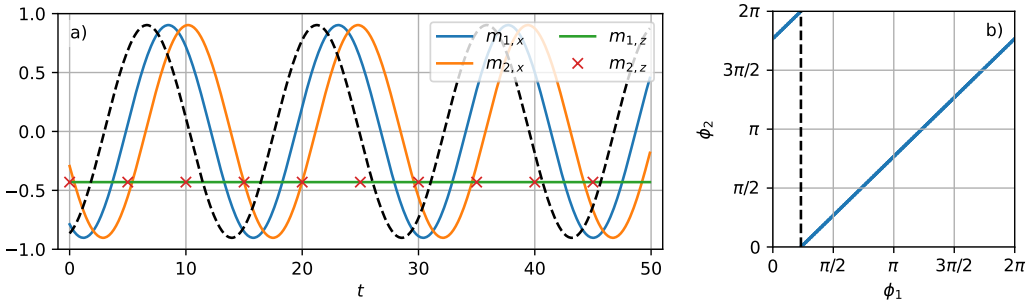

Fig. 4. Synchronous oscillation in the system (4.1) at $\alpha = 0.01$, $\beta_1 = 0.0046$, $\beta_2 = 0.004$ $\epsilon = 0.00045$, $h_z = 0$. The initial values for $\vec{m}_{1,2}$ are specified by Eq. (5.1). (a) Time dependencies of $m_{1,2,x}$ and $m_{1,2,z}$. Components $m_{1,x}$ and $m_{2,x}$ are synchronized and $m_{1,2,z}$ do not oscillate and coincide at $m_{1,2,z} = \cos(\theta) = -0.43$ as predicted by Eq. (4.8). Black dashed line is computed as $\sqrt{1-\cos(\theta)^2}\sin(\omega_s t)$ where $\omega_s = 0.43$ is the frequency of the synchronous oscillations according to Eq. (4.9). (b) Diagram of phases $\phi_{1,2}$. The line ϕ_2 vs ϕ_1 crosses the right edge of the square $[0, 2\pi] \times [0, 2\pi]$ just one time and it crosses the top edge also one time. It indicates $1:1$ synchronization. Vertical dashed line is drawn trough the point where $\phi_2 = 0$ so that the corresponding ϕ_1, i.e., the distance between the vertical axis and the dashed line equals to the phase difference $\psi = \phi_1 - \phi_2$. Exactly as predicted by Eq. (4.7a) it is equal to 0.73.

To distinguish the resulting solutions we compute spans of z components along the trajectories, $Z_{1,2} = \max_t m_{1,2,z} - \min_t m_{1,2,z}$, and colorize points on the (θ_1, θ_2) plane according to the sums $Z_1 + Z_2$ normalized by the maximum. Color bars in the panels of Fig. 3 confirm that a colorful scheme is used. But nevertheless there are only two colors on the plots. It means that only two solutions are observed. The synchronized solution corresponds to the black points where $Z_1 + Z_2 = 0$ since as discussed above z components do not oscillate in the synchronized regime. Another solution is non-synchronized and regardless of the initial point it always has the same span of z components, $Z_1 + Z_2 = \text{const}$, so that all corresponding points are painted in gray.

As one can see from Figs. 3a and 3b if $\theta_1 > \theta_2$ only non-synchronized solution can appear (plain gray area) and when $\theta_1 < \theta_2$ the basins of the two solutions are intermittent. (In these figures $\beta_1 > \beta_2$, and if $\beta_1 < \beta_2$ the picture is transposed.) In more detail this is represented in Fig. 3c. The basins of synchronized (black) and non-synchronized (gray) solutions form diagonal stripes. When coupling strengthen, see Fig. 3b and 3d, the black stripes (synchronized) become wider while the gray ones shrink. Further increase of the coupling strength results in an abrupt switch of the whole plane into black color, i.e., all starting points lead to the synchronized solution.

Now we consider examples of particular trajectories. Let us specify definite initial conditions for the first and second oscillators as $\vec{m}_{1,2}(0) = \vec{v}_{1,2}/\|\vec{v}_{1,2}\|$ where the vectors $\vec{v}_{1,2}$ are selected without taking care of their normalization. Two initial conditions will be considered:

$$\vec{v}_1 = (0.1, -0.1, 0.9), \quad \vec{v}_2 = (-0.2, 0.2, 0.8), \tag{5.1}$$

$$\vec{v}_1 = (0.1, -0.2, 0.001), \quad \vec{v}_2 = (-0.1, 0.3, -0.002). \tag{5.2}$$

Figure 4 is plotted for the initial conditions (5.1). The numerical solution is approximated very well by the formulas (4.8), (4.9). Components $m_{1,z}$ and $m_{2,z}$ do not oscillate and have the same value $m_z = \cos\theta$ computed according to Eq. (4.8), see Fig. 4a. Components $m_{1,2,x}$ (as well as the components $m_{1,2,y}$ that are not shown) oscillate synchronously. Black dashed sine curve demonstrates that the synchronized $m_{1,x}$ and $m_{2,x}$ obey pure sine law with the frequency ω_s, see Eq. (4.9). Figure 4b demonstrates dependence ϕ_2 vs. ϕ_1. The line crosses the right edge of the square $[0, 2\pi] \times [0, 2\pi]$ exactly one time and also it crosses the top edge one time. It means that time dependencies $\phi_1(t)$ and $\phi_2(t)$ have identical slopes so that the oscillations are synchronized $1:1$. Vertical dashed line in Fig. 4b goes through the point where $\phi_2 = 0$ so that its distance to the origin equals to the phase shift $\psi = \psi_1 - \phi_2$. Its value coincides with the one computed according Eq. (4.7a).

Figure 5 is plotted at the same parameters as Fig. 4 but for the initial values (5.2). Unlike the synchronous solution represented in Fig. 4 now oscillations of x and y components are not synchronized. Figure 5a illustrates it showing oscillations of $m_{1,x}$ and $m_{2,x}$. Since we consider here

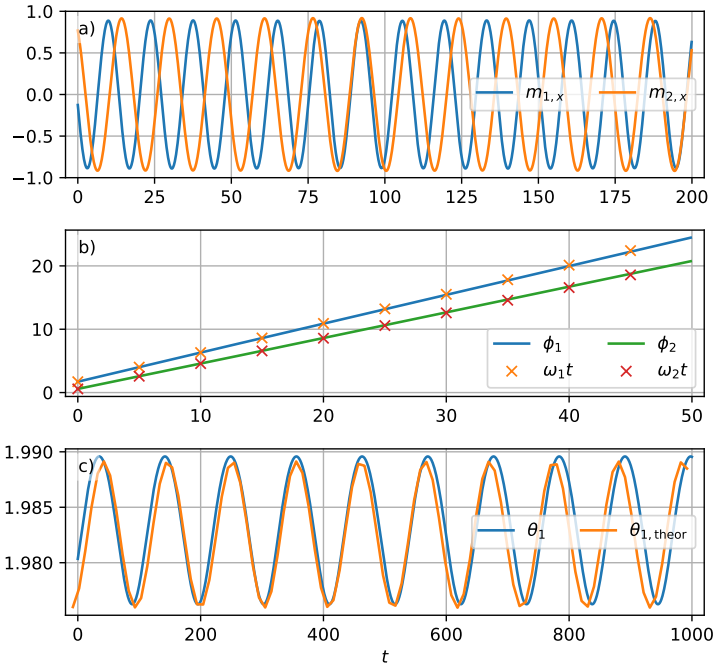

Fig. 5. Non-synchronous oscillations of the system (4.1) at the same parameters as in Fig. 4 but for the initial values (5.2). (a) Time dependencies of $m_{1,2,x}$. Observe different frequencies of the oscillations. (b) Solid lines are unwrapped phases $\phi_{1,2}$. Crosses are plotted according to the formulas $\omega_{1,2}t$ where $\omega_{1,2}$ are the eigenfrequencies of the uncoupled oscillators, see Eq. (2.8). Coincidence of the crosses and the lines indicate that the subsystems frequencies are very close to their eigenfrequencies. (c) Time dependence of θ_1 computed numerically and according to Eq. (4.13), (4.17). Observe high correspondence of the curves.

small coupling strength, the oscillations are very close to sinusoidal with frequencies very close the eigenfrequencies of the uncoupled oscillators, see (2.8). Thus in Fig. 5b time dependences of the unwrapped phases $\phi_{1,2}$ visually indistinguishable from straight lines. The crosses in this figure are plotted according to the formulas $\omega_{1,2}t$. Components z oscillate now with a small amplitude. These oscillations are described well by Eq. (4.13), (4.17). This is illustrated in Fig. (5)c where numerical curve for $\theta_1(t)$ is compared with the theoretical one.

Now we consider examples of parameter planes computed for the permanent initial points (5.1) and (5.2). Two approaches will be used. The first one is based on counting passages of the phases $\phi_{1,2}$ of the top and the right edges of the square $[0, 2\pi] \times [0, 2\pi]$. The ratio of these numbers, so called winding number, indicates the resonance, i.e., the synchronization $m : n$. The second is based on computing Lyapunov exponents spectra at each point of the parameter plane. Totally the system (4.1) has six Lyapunov exponents. But since it preserves the norms of $\vec{m}_{1,2}$ two of the them are always zero. Presence of the positive exponent would indicate chaos, but this is not the case for our system. Situation $\lambda_{1,2} = 0$ and $\lambda_{3,4,5,6} < 0$ indicates fixed point, $\lambda_{1,2,3} = 0$ and $\lambda_{4,5,6} < 0$ mean periodic oscillation and configuration $\lambda_{1,2,3,4} = 0$ and $\lambda_{5,6} < 0$ is observed when the oscillations are quasiperiodic, i.e., the subsystems 1 and 2 are not synchronized.

Figure 6 represents regimes of the system (4.1) in a close vicinity of the point $\beta_1 = \beta_2$. Figures 6a and 6b are the regime charts where the colors indicate winding numbers. For all chart points the same initial conditions are used: those given by (5.1) are used in Fig. 6a and Eq. (5.2) corresponds to 6b. We observe that due to the bistability the charts have different structures. Dashed straight lines marks theoretically predicted boundaries of the bistability area.

Figures 6c and 6d are the Lyapunov exponents charts corresponding the the regime charts above. The initial conditions are again (5.1) and (5.2), respectively. Both regime charts and Lyapunov exponents chart have identical structures that confirms correctness of our computations.

Only two regimes are observed, synchronous and non-synchronous whose examples are represented in Figs. 4 and 5, respectively. The parameters corresponding to these figures are marked by

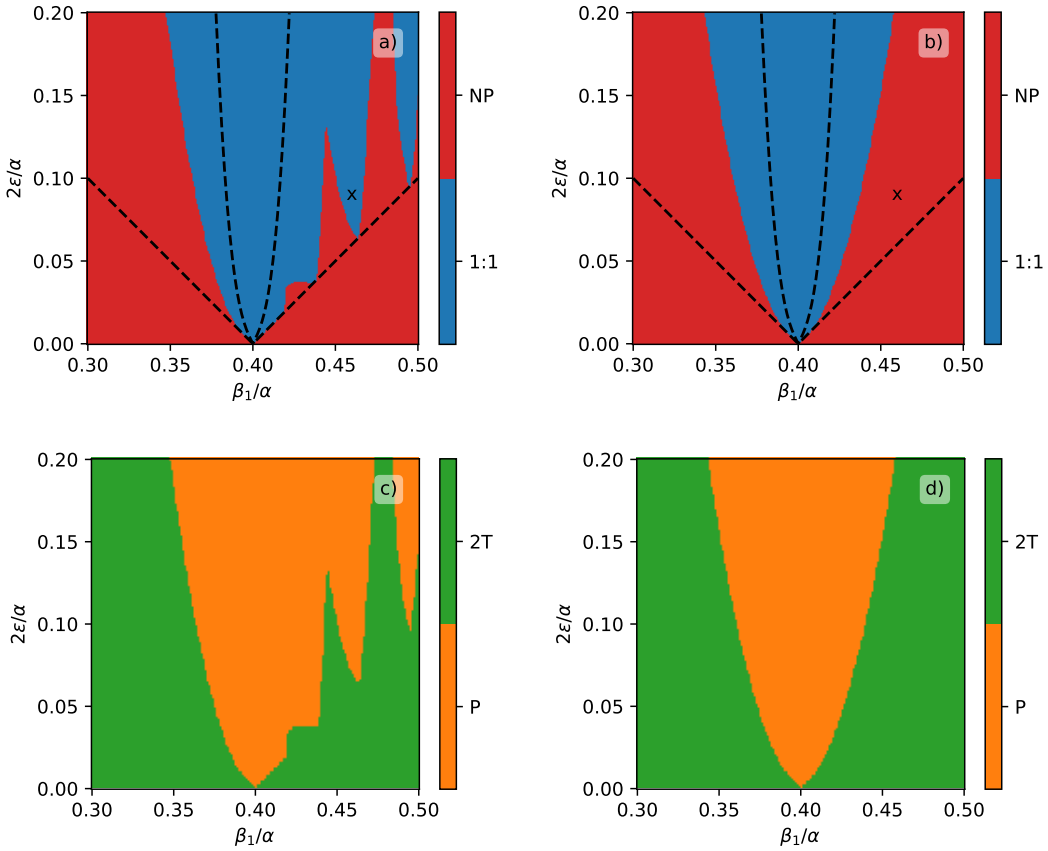

Fig. 6. Regimes of the coupled system (4.1) in a small vicinity of the point $\beta_1 = \beta_2$. $\beta_2 = 0.004$, $\alpha = 0.01$, $h_z = 0$. (a,b) Synchronization charts computed as counts of edges crossings of the square $[0, 2\pi] \times [0, 2\pi]$ by the phase $\phi_{1,2}$, see the explanation of Fig. 4b. Initial values for the charts (a) and (b) are (5.1) and (5.2), respectively. Black dashed lines mark the boundaries of bistability area as predicted theoretically, see Eqs. (4.12) and (4.23). Black cross corresponds to Figs. 4 and 5. Labels are: "NP" — non-periodic, "$1:1$" — synchronization. (c,d) Lyapunov exponents charts. Labels are: "P" — periodic oscillations, "2T" — two-frequency torus.

the black cross in Figs. 6a and 6b. The synchronous oscillations are denoted as "$1:1$" in Figs. 6a and 6b and "P" in Figs. 6c and 6d. It means that we have here periodic oscillations when the oscillator frequencies are equal. Charts for the initial condition (5.1) in Figs. 6a and 6c contains tongue-like strictures of synchronized oscillations whose lower tips are anchored at the lower boundary of the bistability area. This is because the synchronized solution does not exist below this line. We note the all these tongues correspond to $1:1$ synchronization. Non-synchronous oscillations are denoted as "NP" in the regime charts, Figs. 6a and 6b. In actual computations it means that the computed winding number for them includes large integers. In the Lyapunov charts these areas exactly correspond to the areas "2T". It means two-frequency torus, i.e., quasiperiodic regime. We have to notice that the true quasiperiodicity in a strict mathematical sense appears only when the frequency ratio is an irrational number. Obviously not every point in the "2T" areas fulfills this condition. For some of them the frequency ratio is actually rational and hence the oscillations are actually periodic. However the period is very large and the oscillations are indistinguishable from the quasiperiodic ones in numerical simulations without special efforts.

The characteristic feature of the charts in Fig. 6 is their simplicity. Typically on the plane of frequency detuning vs coupling strength there is a structure of tongues anchored at the points where the frequencies ratio is rational, like for example $1:2$, $1:3$, or $2:3$. These tongues emerge due to the effect of phase locking and are usually called Arnold tongues [25]. In our case however the phase locking only occurs at $1:1$. No phase locking of higher harmonics is observed. As we already noticed above this is due to the absence of terms nonlinear in m_x and m_y components in equations for a single oscillator, see Eq. (2.2).

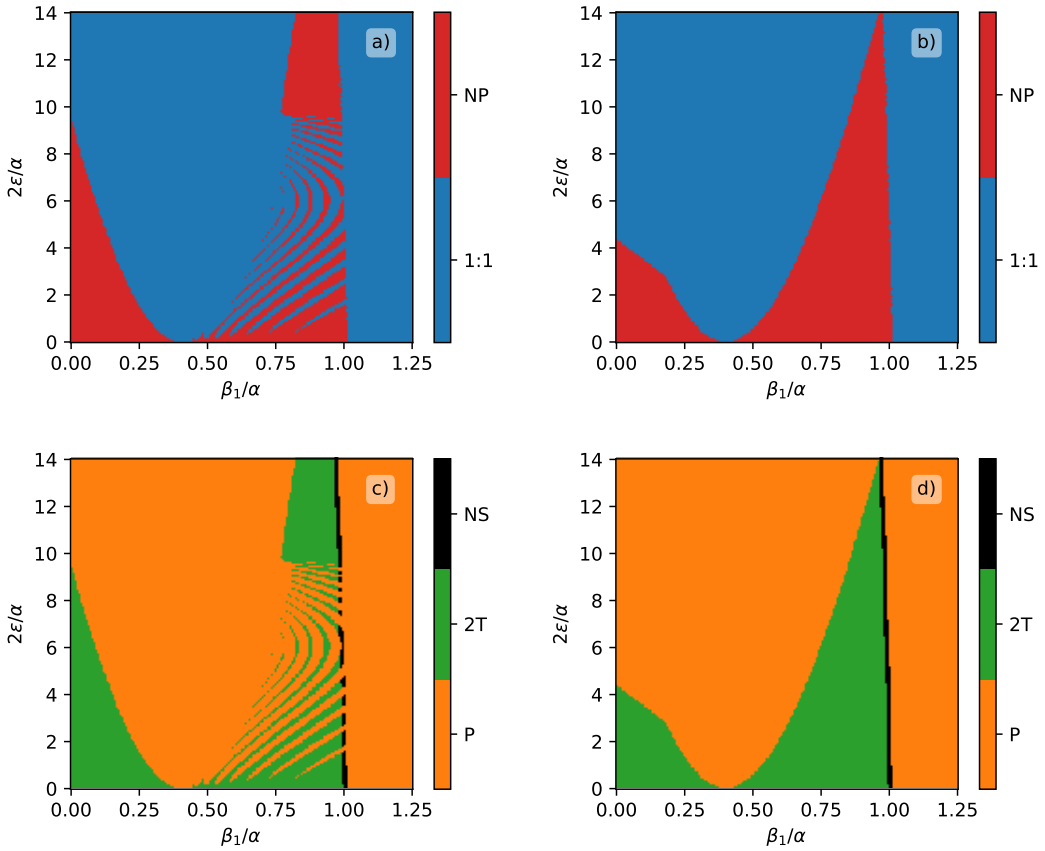

Fig. 7. Same as Fig. 6 for wider ranges of β_1 and ϵ. In panels (c) and (d) black thin areas labeled as "NS" indicate threshold of Neimark-Sacker bifurcation.

Figure 7 demonstrates the charts for wider parameter ranges. Still no complicated structure of Arnold's tongues is observed here. One can find only two regimes describes above. Those tongue-like areas in Figs. 6a and 6c of synchronous oscillations anchored at the lower boundary of the bistability area are developed in Fig. 7a and 7c into patterns that looks like papillary lines. These patterns appear due to the bistability. All chart points are computed for the fixed initial conditions (5.1). When parameter values varies while scanning the chart this initial point falls either to the basin of the synchronous of non-synchronous solution. Thus the pattern appears.

To clarify it better Fig. 8 demonstrates dependence of the three nontrivial Lyapunov exponents $\lambda_{4,5,6}$ vs β_1. (We remind that due to preserving the amplitudes $\|\vec{m}_1\| = \|\vec{m}_2\| = 1$ two of six exponents are always zero, and one more is zero since the system (4.1) is autonomous.) These curves correspond to moving along the horizontal line along the charts in Fig.7 at $\epsilon = 0.01$. Figure 8a is computed when trajectories are started from the initial point (5.1). Jumps of the curves in the right part of the figure correspond to papillary patterns in Fig. 7. One sees that the jumps can be treated as switching between two smooth curves. To reveal these curves explicitly we plot Fig. 8b in the following way. The leftmost point is computed for the initial conditions (5.1) and all subsequent ones when moving to the right are computed when a trajectory start from the previous trajectory end point. One observes the transition to a synchronous periodic regime when λ_4 becomes negative and then this solution undergoes no transformations. The exponents λ_4 and λ_5 coincide in this area due to the full synchronization of the oscillations: both their frequencies and amplitudes are the same, see the example in Fig. 4. The second solution is shown in Fig. 8c. No inheritance is used here, all trajectories start from the initial condition (5.2). This solution undergoes transition to the synchronization in the left part of the curves that corresponds to the synchronization tongue in Fig. 7. Moreover near the point $\beta_1/\alpha = 1$ one observes a scenarios typical for Neimark-Sacker bifurcation [26, 27]. While moving from right to left one observes first a periodic solution. For this

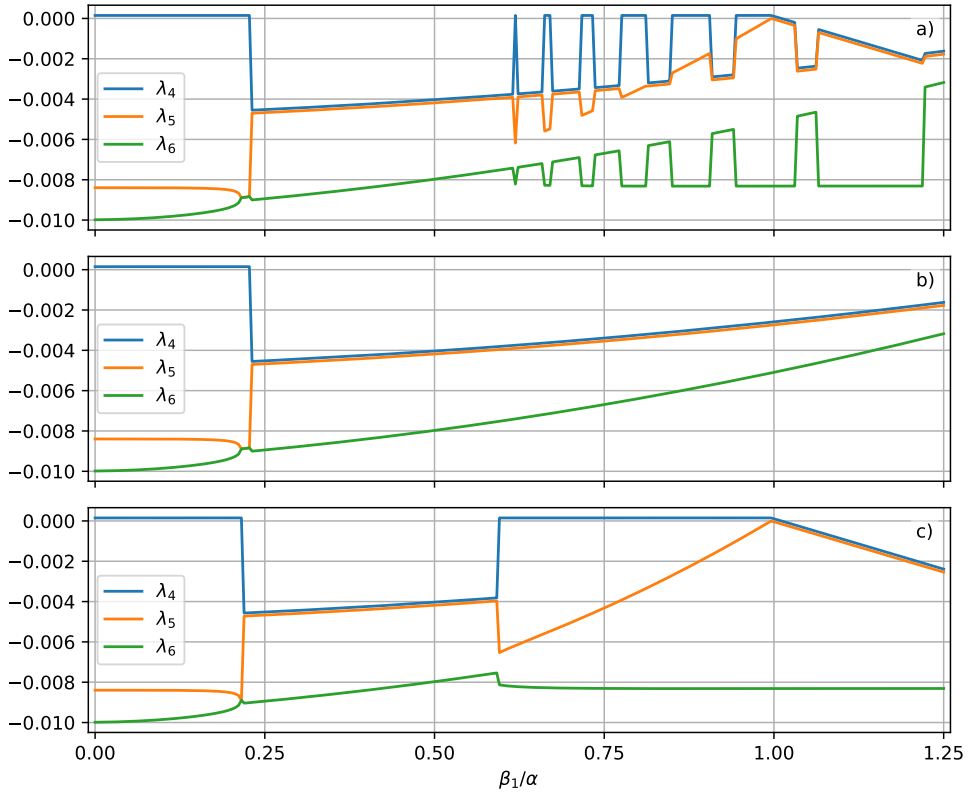

Fig. 8. Lyapunov exponents $\lambda_{4,5,6}$ vs β_1. All parameters are as in Fig. 6, $\epsilon = 0.01$. (a) Initial conditions (5.1). (b) Initial conditions (5.1) for the leftmost point, then inheritance of the initial conditions from left to right. (c) Initial conditions (5.2).

solution $\lambda_4 = \lambda_5$ and both of them negative. Then they approach zero and then only λ_5 becomes negative again. In Figs. 7c and 7d the line of this bifurcation is highlighted with black color.

6. CONCLUSION

The spin transfer oscillator model is three-dimensional and describes precession of a magnetization vector. The length of this vector remains constant so that the dynamics occurs on a sphere and thus is effectively two-dimensional. Generic spin transfer nano-oscillator is described by Landau-Lifshitz-Gilbert-Slonczewski equation that has sufficiently complicated form. In this paper we consider its particular case when the oscillator design is symmetric with respect to z axis. In this case the governing equations are simplified dramatically but nevertheless the system remains physically relevant. When the oscillator is uniaxial the established oscillations occur along a circle of latitude parallel to x-y plane while z component remains constant. Its interesting feature is that when on the limit cycle the governing equations are linear with respect to oscillating components x and y. For a single oscillator it means that oscillations are pure sinusoidal without higher harmonics.

In this paper we analyze how this effective linearity manifests itself when two such oscillators are coupled via magnetic field. Using phase approximation approach we reveal that the system can demonstrate bistability between synchronized and non-scrutinized oscillations. For the synchronized one the Adler equation is derived, and the estimates for the boundaries of the bistability area are obtained. The basins of attraction of the two coexisting solutions are analyzed numerically. Their two dimensional slices consist of sufficiently thin parallel stripes so that a small variation of the initial conditions may result in the switch between synchronized to non-synchronized oscillations.

Charts of regimes and Lyapunov exponents charts are computed numerically. The parameters space of this system has very simple structure. Due to the mentioned effective linearity any higher resonances are absent. Only synchronization with $1:1$ frequency ratio is observed while any other phase locking with a winding number $m:n$, $m > 1$ and/or $n > 1$, never appears.

FUNDING

This work was supported by the Russian Science Foundation, project 21-12-00121, https://rscf.ru/en/project/21-12-00121/

CONFLICT OF INTEREST

The author declares that he has no conflicts of interest.

REFERENCES

1. I. D. Mayergoyz, G. Bertotti, and C. Serpico, *Nonlinear magnetization dynamics in nanosystems* (Elsevier, 2009), ISBN 978-0-0804-4316-4.
2. Z. Zeng, G. Finocchio, and H. Jiang, Nanoscale **5**, 2219 (2013).
3. J. C. Slonczewski, Journal of Magnetism and Magnetic Materials **159**, L1 (1996), ISSN 0304-8853.
4. L. Berger, Phys. Rev. B **54**, 9353 (1996).
5. R. Skomski, *Simple models of magnetism*, Oxford Graduate Texts (Oxford University Press, USA, 2008), ISBN 0198570759.
6. D. Li, Y. Zhou, C. Zhou, and B. Hu, Phys. Rev. B **82**, 140407 (2010).
7. A. Pikovsky, Phys. Rev. E **88**, 032812 (2013).
8. M. A. Zaks and A. Pikovsky, Physica D: Nonlinear Phenomena **335**, 33 (2016), ISSN 0167-2789.
9. M. Zaks and A. Pikovsky, Scientific Reports **7**, 4648 (2017), ISSN 2045-2322.
10. M. A. Zaks and A. Pikovsky, The European Physical Journal B **92**, 160 (2019), ISSN 1434-6036.
11. S. I. Kiselev, J. C. Sankey, I. N. Krivorotov, N. C. Emley, R. J. Schoelkopf, R. A. Buhrman, and D. C. Ralph, Nature **425**, 380 (2003), ISSN 1476-4687.
12. W. H. Rippard, M. R. Pufall, S. Kaka, S. E. Russek, and T. J. Silva, Phys. Rev. Lett. **92**, 027201 (2004).
13. S. Kaka, M. R. Pufall, W. H. Rippard, T. J. Silva, S. E. Russek, and J. A. Katine, Nature **437**, 389 (2005), ISSN 1476-4687.
14. S. M. Rezende, F. M. de Aguiar, R. L. Rodríguez-Suárez, and A. Azevedo, Phys. Rev. Lett. **98**, 087202 (2007).
15. M. Lakshmanan, Philos. Trans. Royal Soc. A **369**, 1280 (2011).
16. A. Slavin and V. Tiberkevich, IEEE Transactions on Magnetics **45**, 1875 (2009).
17. A. Pikovsky, M. Rosenblum, and J. Kurths, *Synchronization.A universal concept in nonlinear sciences* (Cambridge University Press, 2002), ISBN 0-521-59285-2.
18. B. Georges, J. Grollier, M. Darques, V. Cros, C. Deranlot, B. Marcilhac, G. Faini, and A. Fert, Phys. Rev. Lett. **101**, 017201 (2008).
19. D. J. Griffiths, *Introduction to electrodynamics* (Cambridge University Press, 2017), 4th ed., ISBN 978-0-321-85656-2.
20. R. Adler, Proceedings of the IRE **34**, 351 (1946).
21. R. V. Khokhlov, Dokl. Akad. Nauk SSSR **97**, 411 (1954), in Russian.
22. R. V. Khokhlov, IRE Transactions on Circuit Theory **7**, 398 (1960).
23. E. Gengel, E. Teichmann, M. Rosenblum, and A. Pikovsky, Journal of Physics: Complexity **2**, 015005 (2020).
24. M. Kumar and M. Rosenblum, Phys. Rev. E **104**, 054202 (2021).
25. V. S. Anishchenko, V. Astakhov, A. Neiman, T. Vadivasova, and L. Schimansky-Geier, *Nonlinear dynamics of chaotic and stochastic systems: tutorial and modern developments*, Springer Series in Synergetics (Springer, 2007), 2nd ed., ISBN 9783540381648.
26. R. Vitolo, H. Broer, and C. Simó, Nonlinearity **23**, 1919 (2010).
27. R. Vitolo, H. Broer, and C. Simó, Regular and Chaotic Dynamics **16**, 154 (2011), ISSN 1468-4845.